Mathematical Description of the Microstructural Modifications and Changes in the Mechanical Properties during Spheroidization of Medium-Carbon Steel

Sergey Guk, Rudolf Kawalla, and Ulrich Prahl*

A set of experiments is carried out to clarify the microstructure development during an intercritical spheroidization process in AISI 1045 ferritic–perlitic steel, as well as its structure-property relationships at room temperature. Microstructures with a distinctive combination of fine spheroidized carbide particles within a ferrite matrix are created through different heat-treatment combinations. The validation and evaluation of the accuracy of the spheroidizing kinetics and particle coarsening, as well as the prediction of tensile properties of the investigated material, are carried out based on the common empirical and empirical-physical models. Some of the models are then adapted for the material. Quantitative analyses reveals that not all of the model-based predictions correlate well with the experimental measurements. Such instances are associated with the peculiarities of the investigated material.

1. Introduction

The production and processing from a pre-product to a finished part of a material is typically followed by mathematical simulation. This approach allows the properties of the produced workpiece to be predicted. Therefore, the number of models and simulations is constantly growing. Numerous approaches exist in materials science to describe special material properties. As a result, the primary group of these methods consists of models that allow estimations of the mechanical properties.[1,2]

The mechanical behavior of multiphase materials depends on the properties of each individual phase, its geometry and the assembly in the material, that is, its microstructure. Regarding Fe–C alloys, the microstructure can consist of austenite, ferrite, bainite, and martensite. These phases are formed during the cooling and solidification process or during thermal or thermomechanical treatment. The mechanical properties of each phase depend on its chemical composition, technological parameters, and the previous microstructure. Several investigators have researched the association between microstructure and mechanical properties of dual-phase steels.[3–7] A systematic determination of the mechanical properties and their dependence on the microstructure for the efficient development of new materials and optimization of already known materials appears to be feasible.

Spheroidization annealing is a type of heat treatment used to obtain spherical cementite. It is a common example of a technological approach to achieve the necessary mechanical properties of Fe–C alloys with a sufficient tool lifetime through specific modification of the microstructure. The effectiveness of spheroidization annealing depends on the ability of the lamellar cementite within pearlite to transform into a spherical form through the diffusion of carbon. The increasing spheroidization state leads to an increase of the formability and to a decrease of the hardness and strength of the material. Currently, the criterion for a sufficient annealing time is a microstructure with spherical cementite particles with an axial ratio less than 1:3.[8] Therefore, the volume ratio of spherical cementite to its overall volume fraction will be greater than 90%. This volume can also be expressed as the degree of spheroidization. This thermal treatment is often considered the simplest approach; however, a misfit with technical reality is sometimes observed. According to research involving 14 European wire-processing companies from Italy, France, Austria and Germany, approximately 14.7% of defective goods are produced with an improperly designed annealing processes.[9] Currently, because of advances in technology over the past 13 years, material failure rates have decreased. Nevertheless, the main disadvantage of the spheroidization annealing process is its high cost. In general, the process can take longer than 12 h, which can lead to decarburization and scale formation. In addition to these drawbacks, the formation of a microstructure with coarse carbide particles can occur. As result, a final microstructure with some large M_7C_3 precipitates can be observed after the final heat-treatment of hardening and tempering.[10] These precipitates restrain the cyclic fatigue behavior and thus decrease the component's lifetime. A few reports are known for their mathematical descriptions of the microstructural modifications and changes in mechanical properties during spheroidization annealing. The state of

Dr. S. Guk, Prof. R. Kawalla, Prof. U. Prahl
Institute for Metal Forming
TU Bergakademie Freiberg
Bernhard-von-Cotta Straße 4, 09599 Freiberg, Germany
E-mail: sergey.guk@imf.tu-freiberg.de

The ORCID identification number(s) for the author(s) of this article can be found under https://proxylibrary.hse.ru:2120/10.1002/srin.201800335.

DOI: 10.1002/srin.201800335

knowledge about modeling of the spheroidization kinetics and coarsening of cementite as well as the relationship between microstructure and tensile properties is briefly surveyed below.

Regarding the hypothesis that an efficient optimization of spheroidization annealing is possible through quantitative investigations of the spheroidization kinetics and mechanical properties, several authors have dealt with the modeling of spheroidization annealing. All of the described models can be classified into one of two groups: empirical/empirical-physical or physical approaches. Although the physical approaches are based on the Johnson-Mehl-Avrami equation and the Gibbs–Thomson relationship for concentration differences of different particle diameters, the empirical/empirical-physical models correlate the degree of spheroidization E, the mean particle size d, the axis ratio of particle size r, and the mean thickness of non-spheroidized particles x, respectively, with the annealing duration t and annealing temperature T. The relationships of Köstler and Fröhlke (Equation (1)),[11] Dirnfeld and Levin (Equation (2)),[12] and Atasoy and Özbilen (Equation (3))[13] are commonly used:

$$E = m \cdot \lg t + b \tag{1}$$

$$d = a \cdot t^n \tag{2}$$

$$E = 1 - A \cdot \exp\left(-B \cdot r \cdot x^2 \cdot t\right) \tag{3}$$

where m, b, a, A, and B are constants to be determined from the available data.

The spheroidization rate v_E is obtained by the derivation of Equation (1) after the annealing duration:

$$v_E = \left(\frac{dE}{dt}\right)_{\%C;\,\varphi;T} \tag{4}$$

The literature provides several models for predicting the tensile properties of spheroidization-annealed steels. These models are also divided into two groups. The first group contains all empirical-physical relationships, whereas the second group includes micromechanical approaches. The empirical-physical approaches correlate mechanical properties such as lower yield strength R_{eL} and hardness HV, respectively, with the time–temperature parameter P, the mean-intercept ferrite grain size L, and the mean surface-to-surface particle spacing D_s^*. The relationships of Hollomon–Jaffe (Equation (5)),[14] Syn (Equation (6)),[15] and Taleff (Equation (7))[16] are common:

$$P = (C + \ln t) \cdot T \tag{5}$$

$$R_{eL} = 310 \cdot D_S^{*-\frac{1}{2}} \cdot 460 L^{-\frac{1}{2}} \tag{6}$$

$$R_{eL} = (\sigma_0)_{ss} + 145 \cdot D_S^{*-\frac{1}{2}} \cdot 460 L^{-\frac{1}{2}} \tag{7}$$

where $(\sigma_0)_{ss}$ is the contribution from solid-solution strengthening, which is constant for any given group of alloys. Furthermore, C is a constant to be determined from available data.

However, a review of the literature reveals that insufficient information exists about the applicability and interchangeability of the aforementioned methods toward the same material. Thus, the purpose of the present investigation is to conduct such a study. Specifically, a medium-carbon steel containing 0.45% C is investigated. The results are compared with those of studies of other spheroidized steels.

2. Experimental Section

The chemical composition (wt%) of the hot-rolled AISI 1045 carbon steel used in this study was 0.45C, 0.16 Si, 0.69 Mn, 0.05 Cr, 0.023 P, and 0.019 S. Before spheroidization, the experimental steel rods with dimensions $\text{ø}10 \times 100\,\text{mm}^2$ were first austenitized at 900 °C for 0.25 h and then air-cooled to produce a coarse perlitic structure with an interlamellar spacing of 0.55 μm. The mean ferrite grain size was 6 μm.

An intercritical heat-treatment process for spheroidization was applied: the samples were heated to 740 °C, maintained at this temperature for 1 h, then air-cooled to 680 °C and soaked at this temperature for 0, 0.5, 1, 2, 4, 8, 12, 16, or 24 h. Finally, the samples were cooled to room temperature.

After spheroidization, all specimens were polished and etched with 3% Nital solution. For detailed understanding of the microstructural evolution during the heat-treatment, metallographic observations in the longitudinal section were carried out by scanning electron microscopy (SEM). Middle voltage (20 keV) imaging was performed to obtain overview secondary images of the ferrite and cementite with a magnification between 2000× and 3000×. The working distance was approximately 8 mm. The size of ferrite grains was measured by the linear intercept method. The carbide particle sizes showed a bimodal distribution. Hence, two carbide sizes were documented by determining the mean diameter of carbide particles located at grain boundaries and that of carbide particles located at grain interiors. To determine the mean diameter of carbide particles located at the grain interiors, approximately 1500 particles were observed at 10.000× magnification. The carbides fraction at the grain boundaries was substantially lower (≈5%). Therefore, only 400 randomly selected carbide particles were considered under each heat-treatment condition. Particles with an area smaller than $0.001\,\mu\text{m}^2$ were not considered in the analysis. For the evaluation of the mean center-to-center particle spacing, the function "Delayunai Voronoi" in the image analyzer software ImageJ was applied. The cementite particles with an aspect ratio less than 3 were considered to be spheroidized. The area ratio of such particles to its overall area fraction represented the degree of spheroidization. Here, the aspect ratio was defined as the ratio between the maximum and minimum lengths of the cementite particles.

To evaluate the strength and formability of the steel, tensile tests were conducted at room temperature with a constant cross-head speed of $3\,\text{mm}\,\text{min}^{-1}$ using an AG100 uniaxial material testing machine. Cylindrical samples with a gauge diameter of 4 mm and a gauge length of 20 mm were used. Furthermore, the mechanical properties were evaluated by low-force hardness measurements using a Vickers indenter with an applied load of 1 kg.

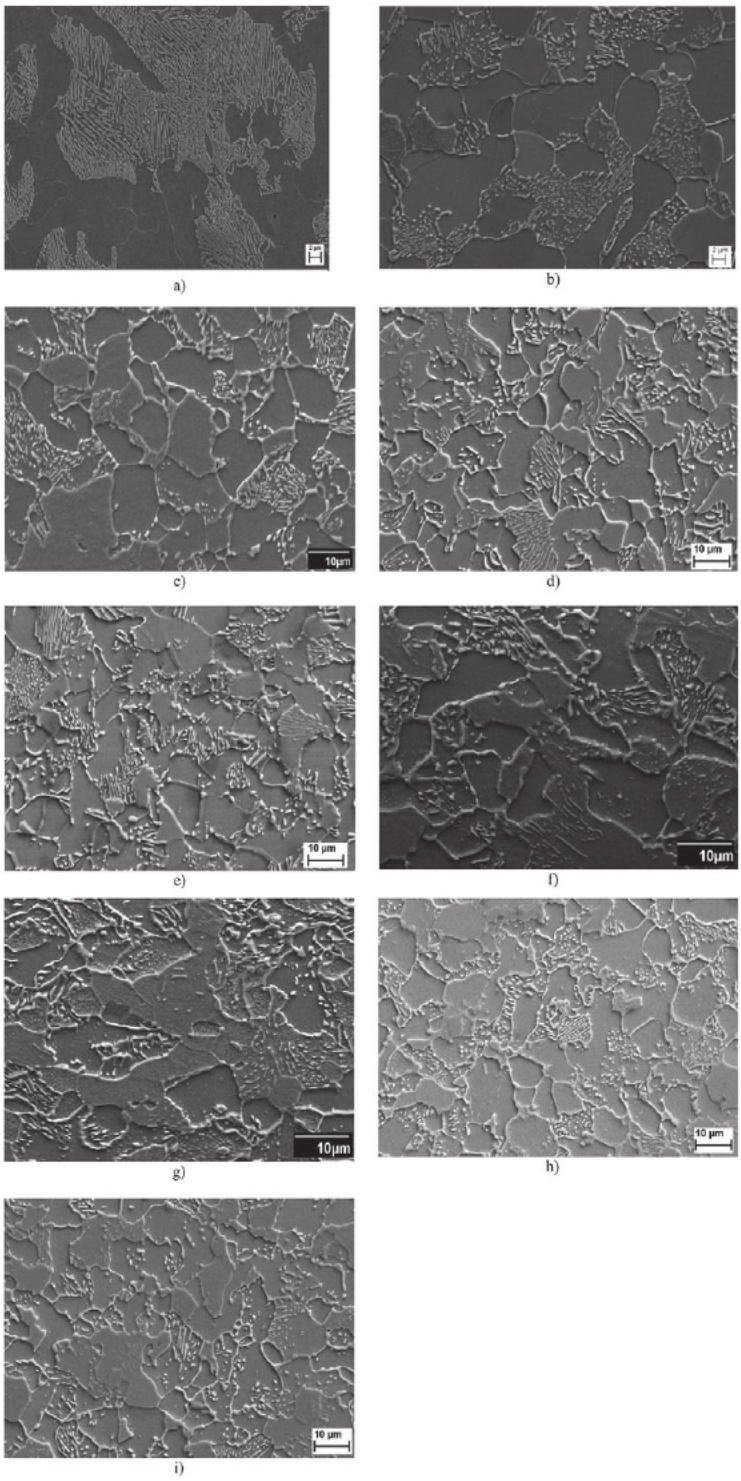

Figure 1. SEM micrographs (SE and BSE mode) of the structure of the AISI 1045 steel after soaking at 680 °C for 0 a), 0.5 b), 1 c), 2 d), 4 e), 8 f), 12 g), 16 h), and 24 i) h.

3. Results

The microstructures resulting from each heat treatment of AISI 1045 are shown in **Figure 1**. Evaluation of the micrographs shows that the lamellar perlite has not yet been completely spheroidized into globular cementite after 8 h of annealing. In addition to areas already spheroidized, areas that clearly still have lamellar perlite are observed. However, these areas can only be spheroidized with even longer annealing times, leading to further strong coarsening of some large cementite particles. After 12 h of annealing, no lamellar perlite was present in the microstructure. Thus, strong coarsening of cementite particles during longer annealing times was not observed.

The evolution of the aspect ratio of cementite particles for different spheroidization times is illustrated in **Figure 2**. The aspect ratio values for an annealing time of 0 h ranged from 3:1 to 60:1. With increasing treatment time, the total number of class intervals substantially decreases. Notably, the final aspect ratio values for the annealing time of 24 h ranged from 3:1 to 20:1; that is, some particles did not reach a spheroidized condition.

In **Table 1**, the microstructural parameters and mechanical properties for all of the heat-treatment conditions employed in this investigation are summarized. The listed microstructural parameters include the mean-intercept ferrite grain size L, mean particle diameter of intra-grain carbides d_{ig}, mean particle diameter of grain-boundary carbides d_{gb}, mean center-to-center particle spacing D_s, and the degree of spheroidization E. The mechanical properties listed in Table 1 are the lower yield strength R_{eL}, ultimate tensile strength R_m, hardness $HV1$ and the reduction of area Z.

4. Discussion

4.1. Spheroidization Kinetics and Coarsening of Cementite

The spheroidization kinetics of cementite particles in the medium-carbon steel with a ferrite–pearlite microstructure was first investigated using the model of Köstler (see Equation (1)). **Figure 3** shows the results of the spheroidization evaluation as a function of the annealing time. The data are from the present investigation as well as from Köstler[17] for an AISI 1035 steel after normalization annealing at 847 °C for 30 min and two different spheroidization annealing temperatures of 650 and 700 °C. In contrast to the heat treatment in the present investigation, that by Köstler was carried out in the form of a subcritical heat-treatment process. The logarithm of the annealing time and the degree of spheroidization exhibit a linear relationship with very good correlation. In this investigation, cementite spheroidization already occurred during the partial transformation that occurs just above the Ar_1 temperature. This observation reflects the high initial degree of spheroidization, as already reported in detail.[18] The equations of the equalizing lines passing through the points are also shown in Figure 3. From these results, we

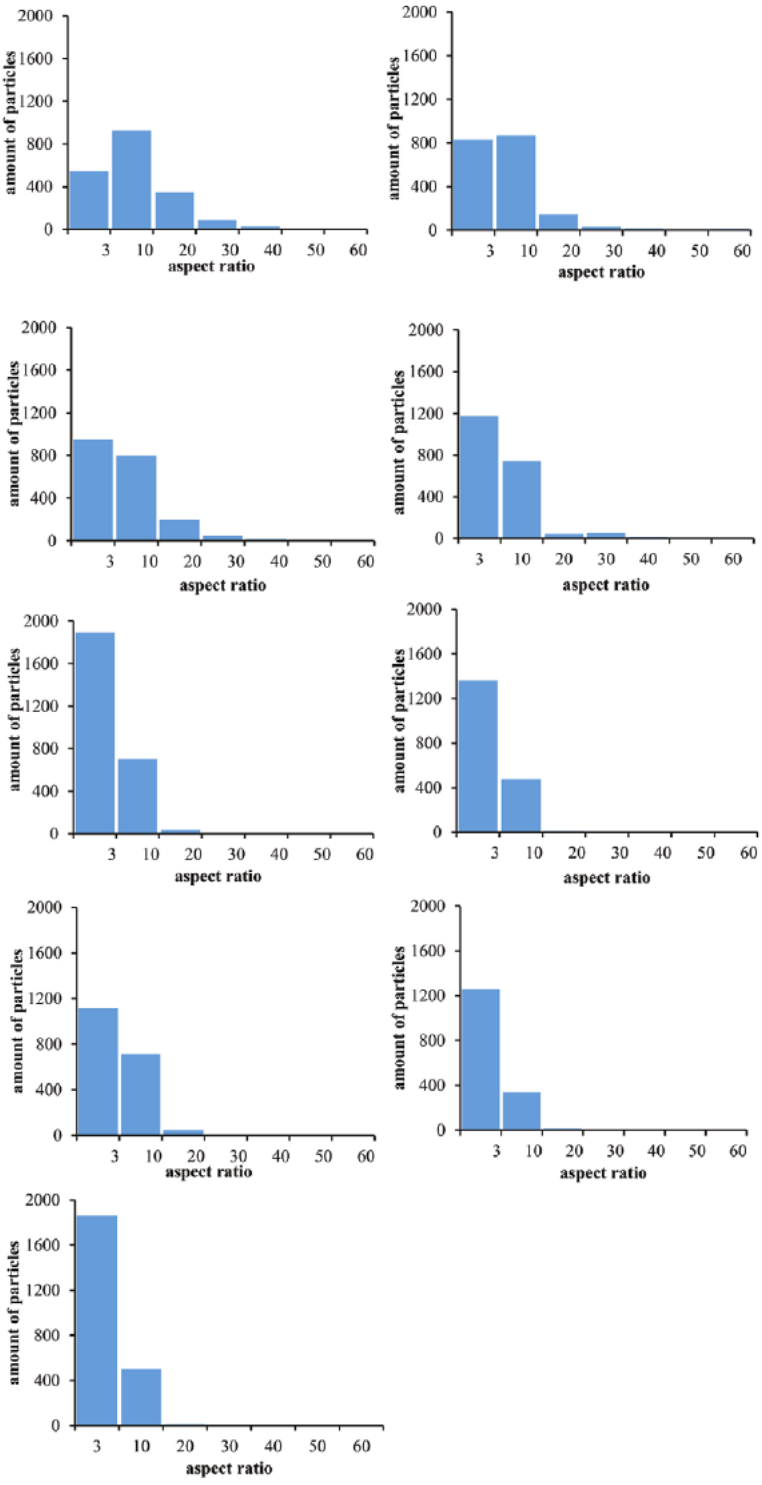

Figure 2. Cementite particle distributions as a function of the aspect ratio after soaking at 680 °C for 0 a), 0.5 b), 1 c), 2 d), 4 e), 8 f), 12 g), 16 h), and 24 i) h.

deduced that the rate of the cementite spheroidization is the slowest in our investigation. As reported,[11] the values m and b of Equation (1) depend on the pearlite interlamellar spacing, the deformation degree of pre-forming and the annealing temperature. However, they are independent of the change in carbon content in the range from 0.15 to 0.60% C for unalloyed steel grades during annealing without pre-forming. Despite the absence of information about prior microstructure in ref. [17], we assumed based on Figure 3 that the pearlite interlamellar spacing in the steel from our investigations was greater. The fine pearlite has a shorter diffusion distance and therefore will spheroidize more quickly than a coarse pearlite microstructure.

The coarsening kinetics of cementite particles was calculated according to the Dirnfeld approach (see Equation (2)). To determine the mean particle diameter d at time t, the relationship proposed by Liu and Gurland[19] was used. It describes the link between the measured center-to-center particle spacing D_s, the mean particle diameter d, and the volume fraction of second phase f (iron carbide in the present case):

$$D_S = \left(\frac{2}{3f}\right)^{1/2} \cdot d \cdot (1-f) \tag{8}$$

For the investigated steel, $f = 0.072$. The coarsening exponent n was determined according to the slope of the lines shown in **Figure 4**. The log–log plot of the mean particle diameter and annealing time shows a good correlation in the form of a linear relationship. The measured n value of the investigated steel is 0.30. The nearly same coarsening exponent n can also be determined based on the data from ref. [12] for a eutectoid steel with 0.89% C and a low Al-content, where the steel was heat treated after undergoing normalizing annealing by subcritical spheroidization annealing at a similar temperature range (see Figure 4). Some authors have reported that the exponent n is a function for controlling the coarsening mechanism. The introduced coarsening kinetics are as follows: $n = 0.33$ for matrix diffusion,[20,21] $n = 0.25$ for boundary diffusion,[22,23] and $n = 0.20$ for diffusion along dislocations.[23,24] Meanwhile, Lindsley and Marder[24] proposed that the coarsening of cementite particles proceeds by a combination of different coarsening mechanisms. Therefore, in the investigated steel, the cementite coarsening occurs in all possible ways by a combination of matrix and boundary diffusion.

The next possibility to describe the spheroidization kinetics is the model according to Atasoy (see Equation (3)). Atasoy proposed an exponential equation for spheroidization during subcritical heat treatment for a steel with 0.59% C and a mean interlamellar spacing of 0.57 µm. Atasoy proposed that, because spheroidization involves the pinching off of lamellae, the coefficient B is defined as the rate of lamellae of aspect ratio r pinching off per unit time per unit unspheroidized area. Atasoy defined the spheroidization rate k as $k = B \cdot r \cdot x^2 \cdot t$. He plotted values of $\ln\left(\frac{f}{f_{\alpha}}\right)$ versus time and measured the k values. In the present work, $f = 0.072$ is the

Table 1. Measured microstructural characteristics and mechanical properties of 1045 steel.

Spheroidization time [h]	L [µm]	d_{ig} [µm]	d_{gb} [µm]	D_s [µm]	E [%]	R_{eL} [MPa]	R_m [MPa]	$HV1$ [–]	Z [%]
0	6.5	0.16	0.31	0.45	7	404	622	192	59
0.5	7	0.26	0.41	0.74	43	366	555	164	61
1	7.7	0.31	0.47	0.88	47	356	549	161	62
2	9.2	0.68	0.84	1.91	59	351	546	156	63
4	9.4	0.65	0.88	1.84	60	349	540	154	64
8	9.5	0.65	1.06	1.83	71	348	537	154	64
12	9.7	0.7	1.15	1.96	73	348	530	152	64
16	9.8	0.71	1.17	1.99	76	345	529	152	64
24	10.3	0.74	1.14	2.1	78	342	518	147	64

constant total carbide volume fraction and f_u is the unspheroidized volume fraction $\frac{f}{f_u} = \frac{1}{1-E}$. **Figure 5** (left) presents such a diagram for the data in this investigation and for the Atasoy data. The plotted values of $ln\left(\frac{f}{f_u}\right)$ do not correlate well with time, especially the results of the current investigation. Furthermore, the carbide spheroidization in the case of the examined steel 1045 is much faster than that in the material investigated by Atasoy. The difference in the spheroidization rate can be partly attributed to the different heat-treatment processes used[18] and the different C-contents. In Figure 5 (right), the relationship between spheroidization time and spheroidization degree is presented, as calculated on the basis of Equation (3) and Figure 5 (left). The calculated values of spheroidization degree E for the investigated steel 1045 do not agree with the measured values (see Table 1). This lack of agreement show that the Atasoy model cannot be used for the experimental conditions in the present work.

4.2. Relationship between Microstructure and Tensile Properties

Liu and Gurland[19] showed that the fracture strength correlates well with the reciprocal of the square root of the mean carbide particle diameter. Since this mechanical property is very rarely included in the characterization of a material, we evaluated whether a correlation exists with the lower yield strength, the tensile strength and the reduction of area. In addition, almost all studies thus far have considered the relationship of strength with only the dominant diameter of cementite particles. This relationship is typical for the microstructure obtained via quench-and-temper processing. In the present investigation, however, two distinct carbide diameters should be considered: the fine carbides located at grain interiors and the coarse carbides located at grain boundaries. **Figure 6** plots the lower yield strength, the tensile strength, and the reduction of area, and two distinct carbide diameters are shown. A better correlation with the mechanical properties was obtained for the case of the carbide diameter at grain interiors. Sufficient correlation with the reduction of area values implies that, in the case of the investigated steel, the high volume content of carbides of approximately 98% located at grain interiors is related to the fracture. Voids or cracks formed during plastic deformation of spheroidized steels are typically observed at carbide particles.[25]

The next possibility to examine the relationship between microstructure and tensile properties is to use the Hollomon-Jaffe parameter. According to the relationship of Hollomon-Jaffe, the hardness of a microstructure is directly proportional to a parameter P, which is a function of tempering temperature and time, as given by Equation (5). Parameter C is a constant and depends on the chemical composition of the steel. Kang and Lee[26] proposed a relation between the alloying element effect and the constant C:

$$C = k_0 + \sum_i k_i X_i \tag{9}$$

where k_i is the coefficient for the alloying element i, X_i is the amount of alloying element in mass%, and k_0 is a constant related to the tempering of pure iron. The composition-dependent C of 1045 steel calculated according to Equation (9) is 12.69. **Figure 7** (left) shows the measured hardness with the tempering parameter using a calculated constant $C = 12.69$ and the composition-dependent tempering parameter from Equation (5), respectively. The data are from the present investigation and from Jusevic et al.[27] for a high-strength low-alloyed steel with a composition (wt%) of 0.30C, 0.90 Si, 0.98 Mn, and

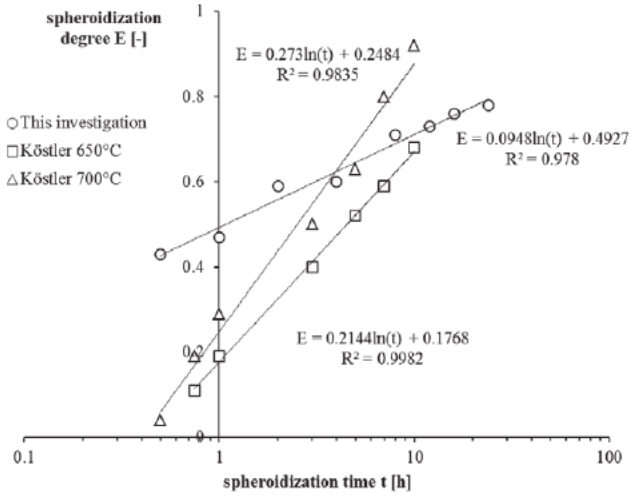

Figure 3. Relationship between the spheroidization time and spheroidization degree according to Köstler (see Equation (1)).

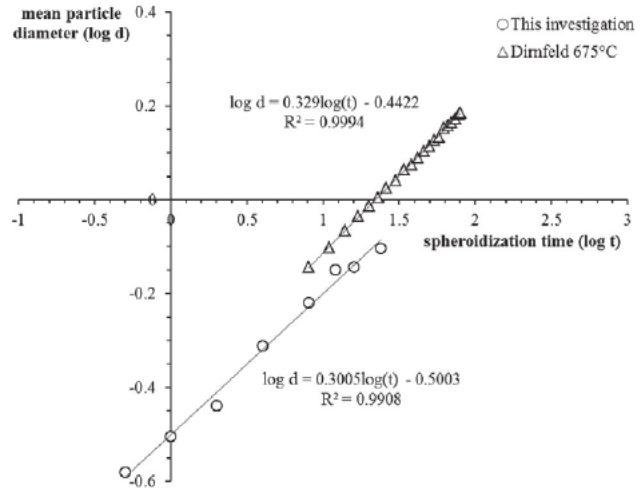

Figure 4. Relationship between the spheroidization time and the mean particle diameter according to Dirnfeld (see Equation (2)).

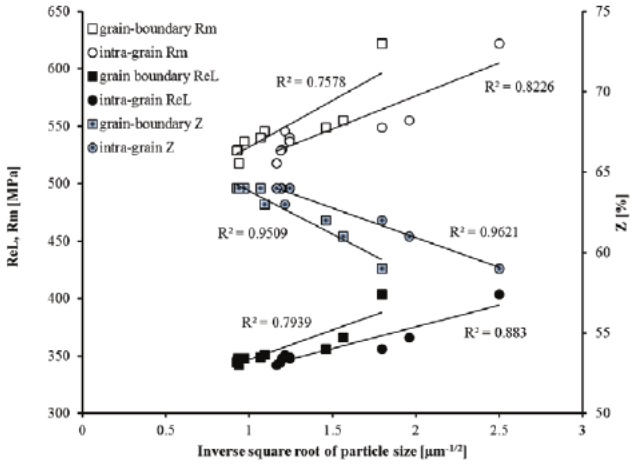

Figure 6. The lower yield strength, tensile strength and the reduction of area plotted against the inverse square root of the mean particle diameter of the grain interior and the grain-boundary carbides.

1.0 Cr after quenching at 870 °C and annealing at two different temperatures of 600 and 650 °C for 0.25 to 24 h. Despite the different hardness values due to the different chemical compositions of the steels, the measured hardness values decrease with increasing tempering parameter. The linear relationships show a good correlation. In Figure 7 (right), the evolution of mechanical properties with increasing tempering parameter P is presented. The mechanical properties R_m and Z show sufficient correlation with parameter P, and the prediction of the lower yield strength R_{eL} is not sufficiently accurate. This fact reflects the effect of interchangeability of processing parameters such annealing temperature and time on these tensile properties. That is, these results indicate that the applied spheroidization regimes with similar values of parameter P will provide almost identical values of tensile strength and a reduction of area. We concluded that the Hollomon-Jaffe parametric Equation (5) well describes the change of mechanical properties depending on the tempering parameter.

Recently, Syn and Taleff suggested a semi-empirical equation to predict the lower yield strength of spheroidized steels with a wide range of chemical compositions (see Equation (6) and (7)). They reported a good prediction accuracy of the developed models. In the case of the examined 1045 steel, the contribution from solid-solution strengthening $(\sigma_0)_{ss}$ is 20 MPa.[16] **Figure 8** compares the prediction accuracy using three different models: those of Syn (Equation (6)), Taleff (Equation (7)), and Hollomon-Jaffe (Equation (5)). The lower yield strength calculated on the basis of the

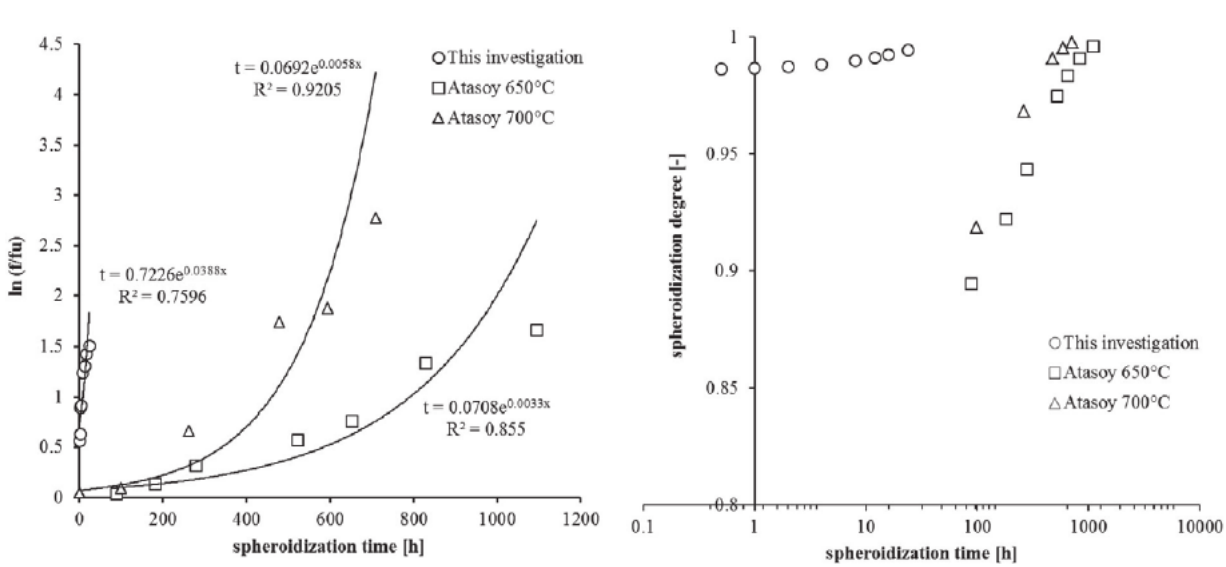

Figure 5. Ratio of the total carbide volume/unspheroidized carbide volume plotted against time (left), and the relationship between the spheroidization time and the spheroidization degree (right) according to the model of Atasoy (see Equation (3)).

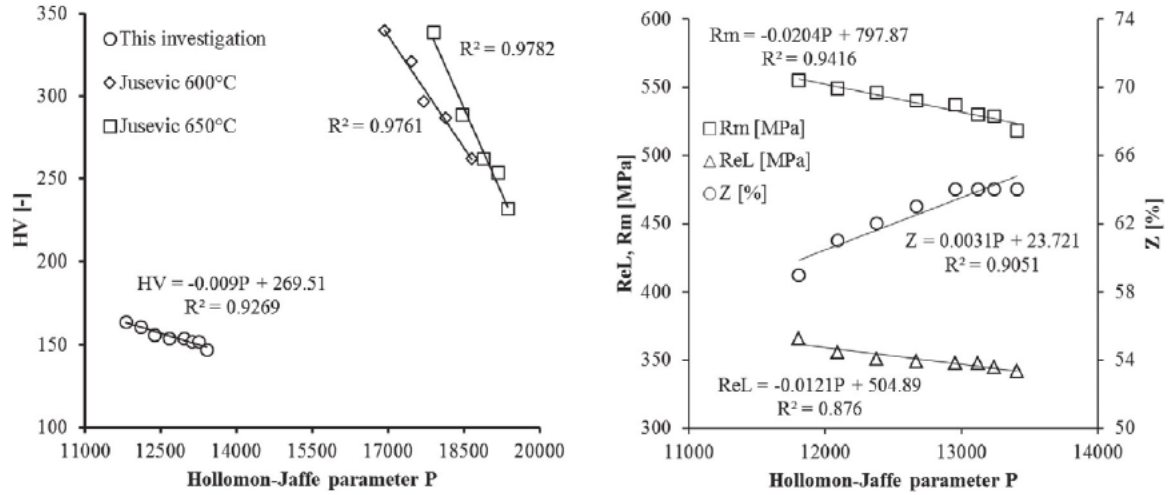

Figure 7. Relationship between the Hollomon-Jaffe parameter *P* and mechanical properties of the 1045 steel (see Equation (5)).

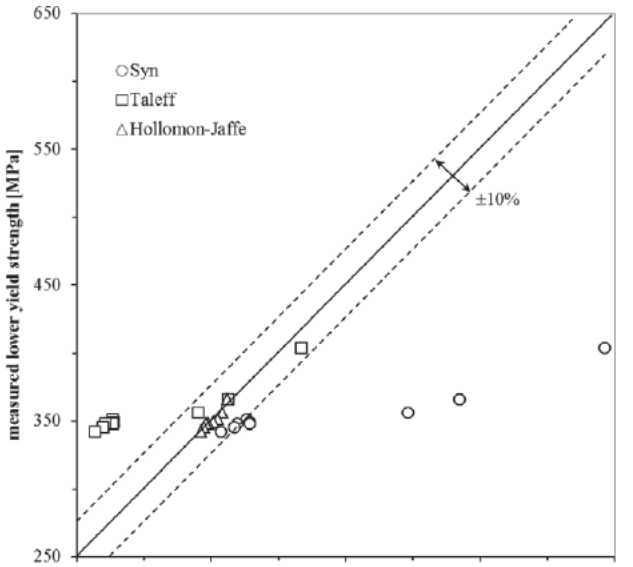

Figure 8. Predicted lower yield strength compared with the experimental data in **Table 1**.

Hollomon-Jaffe relationship shows higher accuracy than the yield strengths calculated on the basis of the other two models.

5. Conclusions

Based on a literature overview and obtained experimental results, for the investigated ferriti–perlitic steel AISI 1045 with initial interlamellar spacing of 0.55 μm, the prediction accuracy of the spheroidizing kinetics and mechanical properties after interrupted intercritical heat-treatment spheroidization process was carried out. This prediction used common empirical and empirical-physical models. Some of the models were subsequently adapted for the material. The following conclusions are drawn from this work:

1) The maximum applied annealing time of 24 h was not sufficient for a complete spheroidization of the cementite.
2) The factors controlling the coarsening kinetics during intercritical annealing in the investigated steel were found to be a combination of matrix and boundary diffusion.
3) The best match for the prediction of the spheroidization kinetics was shown by the approach of Dirnfeld. For the other models considered, deviations are attributable to their substantially higher sensitivity to the applied heat-treatment process and the C-content.
4) An equally strong influence of the cementite particles located at grain boundaries and at grain interiors on the reduction of area of the steel was observed.
5) We concluded that the Hollomon–Jaffe parametric equation gives the best prediction of the changing mechanical properties. Other models lead to serious deviations due to the substantially higher sensitivity to the C-content.

Acknowledgements

Sincere thanks go to Ms. Eva Augenstein from the Fraunhofer Institute for Mechanics of Materials IWM, Freiburg, for the SEM investigations and to Ms. Anna Kowalska and Ms. Estera Kotas for carrying out the quantitative metallography analysis.

Conflict of Interest

The authors declare no conflict of interest.

Keywords

cementite spheroidization, coarsening, hypoeutectoid steel, kinetics, mechanical properties

Received: June 27, 2018

Revised: September 19, 2018

[1] J. Bouquerel, K. Verbeken, B. C. De Cooman, *Acta Mater.* **2006**, *54*, 1443.
[2] G. Krauss, *Steels: Processing, Structure, and Performance*, ASM International, Ohio, USA **2005**.
[3] R. Bakhtiari, A. Ekrami, *Mater. Sci. Eng. A* **2009**, *525*, 159.
[4] S. Guk, *Freiberg. Forschungsh.* **2006**, *B*, 335.
[5] A. Bag, K. K. Ray, E. S. Dwarakadasa, *Met. Mater. Trans. A* **1999**, *30A*, 1193.
[6] M. Sarwar, R. Pristner, *J. Mater. Sci.* **1996**, *31*, **2091**.
[7] N. J. Kim, G. Thomas, *Met. Trans. A* **1981**, *12A*, 483.
[8] T. Das, J. Y. Li, M. Painter, E. Summerville, *J. Mater. Eng. Perform.* **2002**, *11*, 86.
[9] C. Mapelli, R. Venturini, M. Boniardi, *Scand. J. Metall.* **2005**, *34*, 192.
[10] C. Wu, V. Sahajwalla, P. Krauklis, *ISIJ Int.* **1996**, *36*, 347.
[11] H. J. Köstler, M. Fröhlke, *Arch. Eisenhüttenwesen* **1975**, *46*, 655.
[12] S. F. Dirnfeld, L. Levin, *HTM* **1972**, *27*, 12.
[13] Ö. E. Atasoy, S. Özbilen, *J. Mater. Sci.* **1989**, *24*, 281.
[14] J. H. Hollomon, C. D. Jaffe, *Transactions AIME* **1945**, *42*, 223.
[15] C. K. Syn, D. R. Lesuer, O. D. Sherby, *Metall. Mater. Trans. A, Phys. Metall. Mater. Sci.* **1994**, *25A*, 1481.
[16] E. M. Taleff, C. K. Syn, D. R. Lesuer, O. D. Sherby, *Metall. Mater. Trans. A, Phys. Metall. Mater. Sci.* **1996**, *27A*, 111.
[17] H. J. Köstler, *Arch. Eisenhüttenwesen* **1975**, *46*, 229.
[18] S. Guk, D. Hoppach, R. Kawalla, *Key Eng. Mater.* **2017**, *746*, 161.
[19] C. T. Liu, J. Gurland, *Trans. TMS-AIME* **1968**, *242*, 1535.
[20] S. K. Das, A. Biswas, R. N. Ghosh, *Acta Metall. Mater.* **1993**, *41*, 777.
[21] R. T. DeHoff, C. V. Iswaran, *Met. Trans. A* **1982**, *13*, 1389.
[22] K. M. Vedula, R. W. Heckel, *Met. Trans.* **1970**, *1*, 9.
[23] A. J. Ardell, *Acta Metall.* **1972**, *2*, 601.
[24] B. A. Lindsley, A. R. Marder, *Acta Mater.* **1998**, *46*, 341.
[25] Y. Ohashi, J. Wolfenstine, R. Koch, O. D. Sherby, *Mater. Sci. Eng. A* **1992**, *151*, 37.
[26] S. Kang, S. Lee, *Mater. Trans.* **2014**, *55*, 1069.
[27] Z. Jusevic, Z. Gulisija, M. Mihailovic, A. Pataric, *Chem. Ind. Chem. Eng. Q.* **2009**, *15*, 131.

